Preprint typeset in JHEP style - HYPER VERSION arXiv:1004.3056

Systematic effects in the extraction of the 'WMAP haze'

Philipp Mertsch & Subir Sarkar

Department of Physics, University of Oxford, 1 Keble Road, Oxford OX1 3NP, UK
E-mail: p.mertsch@physics.ox.ac.uk, s.sarkar@physics.ox.ac.uk

Abstract: The extraction of a 'haze' from the WMAP microwave skymaps is based on subtraction of known foregrounds, *viz.* free-free (bremsstrahlung), thermal dust and synchrotron, each traced by other skymaps. While the 408 MHz all-sky survey is used for the synchrotron template, the WMAP bands are at tens of GHz where the spatial distribution of the radiating cosmic ray electrons ought to be quite different because of the energy-dependence of their diffusion in the Galaxy. The systematic uncertainty this introduces in the residual skymap is comparable to the claimed haze and can, for certain source distributions, have a very similar spectrum and latitudinal profile and even a somewhat similar morphology. Hence caution must be exercised in interpreting the 'haze' as a physical signature of, *e.g.,* dark matter annihilation in the Galactic centre.

Keywords: Cosmic Microwave Background Radiation, Galaxies, High Energy Astrophysics.

1. Introduction

The measurement of anisotropies in the cosmic microwave background (CMB) by COBE and WMAP has ushered in an exciting new era in cosmology. The study of the cosmic signal requires careful subtraction of galactic foreground emissions and this will become even more crucial for studies of the 'B-mode' polarisation signal by PLANCK and the proposed CMBPol satellites [1]. It is interesting in this context that the subtraction of all known foregrounds, *i.e.,* free-free (bremsstrahlung), thermal dust and synchrotron (as well as the CMB), from the WMAP skymaps leaves an anomalous emission — the "WMAP haze" [2]. This has a roughly spherical morphology localised around the centre of the Galaxy, and a harder spectrum [3] than synchrotron radiation by relativistic cosmic ray (CR) electrons from standard astrophysical sources like supernova remnants (SNRs). An independent analysis has confirmed the existence of the haze [4], but others do not find the evidence to be significant [5, 6].

It was believed initially that the haze is free-free emission from ionised gas too hot to be traced by recombination line maps but too cold to be visible in X-rays [2]. However it was suggested later that it is in fact synchrotron emission from a new population of relativistic electrons,[1] produced by dark matter annihilation [7]. It is indeed thus possible to explain the haze [8] although other authors argue that the annihilation cross-section needs to be significantly boosted over the usual estimate for thermal relic dark matter [6]. There have also been attempts to fit both the morphology and spectrum of the haze by ascribing it to electrons emitted by pulsars with a hard spectrum [9, 10]; however the expected haze is then less spherical since most pulsars are in the galactic disk. This is also true of SNRs which have in fact recently been invoked [11, 12] as sources of positrons with a hard spectrum to explain the rise in the cosmic ray positron fraction at high energies measured by PAMELA [13].

The presence of an additional population of relativistic electrons in the galactic centre appears to be supported by a recent analysis [14] of the γ-ray sky as observed by Fermi-LAT [15]. It is argued that an excess over known components is also present in γ-rays, most likely due to inverse-Compton scattering (ICS) by relativistic electrons, and that the underlying electron distribution is compatible with the WMAP haze [14]. While a signature in ICS is naturally expected if there is indeed an additional population of electrons with a hard spectrum, it was pointed out [16] that some template maps applied in this analysis [14] are in fact inappropriate and underestimate both the π^0 decay and ICS contributions to the γ-ray emission, in particular in the galactic centre region. The analysis in Ref. [14] using the Fermi diffuse model that is believed to be a better tracer of π^0 decay and ICS, however, again shows a residual. The Fermi itself collaboration has not claimed any excess in the galactic centre region over the standard diffuse γ-ray background [17, 18].

A crucial ingredient of both studies [2, 4] that identify a microwave haze is the extrapolation of the morphology of the synchrotron radiation template from 408 MHz to the WMAP bands at 23 (K), 33 (Ka), 41 (Q), 61 (V) and 94 (W) GHz, *i.e.* over two orders of magnitude in frequency. In fact the spatial distribution of the radiating CR electrons is

[1] Here and in the following we use "electrons" when referring to both electrons and positrons.

likely to differ significantly given their energy dependent diffusive transport in the Galaxy. Instead of attempting such a bold extrapolation, other studies, including the analysis by the WMAP collaboration [19], employ the K-Ka difference map as a tracer of synchrotron emission (despite some contamination by free-free emission and an anomalous component which has been interpreted (see, *e.g.,*[20]) as spinning dust [21]). However although both maps are dominated by synchrotron radiation, such a template could also contain any unidentified radiation, such as a possible haze, and therefore cannot exclude it.

CR transport in the Galaxy is dominated by diffusion through interstellar magnetic fields with an *energy-dependent* diffusion coefficient $D(E) = D_0 E^\delta$ where $\delta = 0.3 \ldots 0.7$ [22]. Taking the energy loss rate $b(E) = \mathrm{d}E/\mathrm{d}t = b_0 E^2$ as is appropriate for synchrotron and ICS, the diffusion length ℓ is

$$\ell(E) \approx 5 \left(\frac{E}{\mathrm{GeV}}\right)^{(\delta-1)/2} \mathrm{kpc}\,,$$

for the standard values $D_0 = 10^{28}\,\mathrm{cm^2 s^{-1}}$ and $b_0 = 10^{-16}\,\mathrm{s^{-1}}$ [22]. Therefore, the distance that GeV energy electrons can diffuse is comparable to the Kpc scale on which the source distribution varies; moreover it changes by a factor of 2.4 (1.5) for $\delta = 0.3$ (0.7) in the energy range $\sim 4 - 50$ GeV (corresponding to peak synchrotron frequencies between 408 MHz and 50 GHz for a magnetic field of $6\,\mu$G). As a consequence the $\sim 50\,$GeV electrons will trace the source distribution much better than the $\sim 4\,$GeV electrons which diffuse further away from the sources and wash out their distribution. The synchrotron map at 408 MHz *cannot* therefore be a good tracer of synchrotron radiation at much higher, in particular WMAP, frequencies. Relying on such a crude extrapolation of the morphology of synchrotron emission can thus potentially introduce unphysical residuals. We estimate these by simulating synchrotron skymaps at 408 MHz and the WMAP frequencies and feeding these into the template subtraction process [3]. We show that this leads to residuals of the same order as the claimed haze, which can in fact be matched in spectrum and latitudinal profile for a particular source distribution in the galactic disk. We conclude therefore that the WMAP haze might be an artifact of inappropriate template subtraction rather than evidence of an exotic origin, e.g. dark matter annihilation.

2. Template subtraction

The subtraction method is based on a multilinear regression of the CMB subtracted WMAP data using foreground templates for free-free (f), dust correlated (d) and synchrotron emission (s). Technically this can be achieved by assembling the maps represented each by a vector of all pixels, that is $\mathbf{f}$, $\mathbf{d}$ and $\mathbf{s}$, into one 'template matrix': $P = (\mathbf{f}, \mathbf{d}, \mathbf{s})$. (The template for the haze, $\mathbf{h}$, is appended later.) The pseudo-inverse of P, P^+, allows to determine the coefficients $\mathbf{a} = P^+\mathbf{w}$ that minimise the $\chi^2 = ||\mathbf{w} - P\,\mathbf{a}||^2/\sigma^2$ for the different templates at the WMAP frequencies; σ is the mean measurement noise in each frequency band. For details see Ref. [3].

Since we are interested only in the effect of the electron diffusion on the subtraction of the synchrotron foreground we do not use the free-free and dust templates or radio skymaps

that are strongly affected by local structures such as Loop I [23]. Instead we simulate both the synchrotron skymap at 408 MHz and the skymaps in the WMAP frequency range with the GALPROP code [24]. We adopt the same mask as in Ref. [3] which excises pixels along the galactic plane, around radio sources and in directions of excessive absorption.

To allow comparison with the results of Ref. [3] we apply the same fitting procedure over the whole sky. In order to determine the magnitude of the 'haze' we append a template $\mathbf{h} = (1/\theta - 1/\theta_0)$ to P where $\theta = \sqrt{\ell^2 + b^2}$ is in galactic coordinates and $\theta_0 = 45^\circ$. This corresponds to the "FS8" fit performed in [3] and adding the haze back to the residual maps gives the "FS8 + haze" maps. We determine the latitudinal profile of the residual for $\ell = 0^\circ$ south of the galactic centre direction. As our simulated maps do not contain any localised structures, we do not need to divide the sky into several regions and fit them independently, as was done with the "RG8" fit [3] . We have checked explicitly that doing so does not change the profiles of the residual intensity or the spectral indices.

We have checked that our procedure gives a residual 'haze' in agreement with Ref. [3] when we subtract the 408 MHz survey, the Hα and dust skymaps from the WMAP skymaps. Although with the CMB estimator "CMB5" we find a residual intensity of the same magnitude at 23 GHz, its spectral index of about -0.7 is somewhat softer than in Ref. [3].

3. Diffusion model

The transport of CR electrons is governed by a diffusion-convection equation [25],

$$\begin{aligned}\frac{\partial n}{\partial t} =& \nabla \cdot (D_{xx} \nabla n - \mathbf{v}\, n) + \frac{\partial}{\partial p} p^2 D_{pp} \frac{\partial}{\partial p} \frac{1}{p^2} n \\ & - \frac{\partial}{\partial p} \left(\dot{p}\, n - \frac{p}{3} (\nabla \cdot \mathbf{v})\, n \right) + q\,,\end{aligned}$$

where $n\,\mathrm{d}p$ is the number density of electrons with momentum in $[p, p + \mathrm{d}p]$, $D_{xx} = D_{0xx}(p/4\,\mathrm{GeV})^\delta$ is the spatial diffusion coefficient, $\mathbf{v}$ is the convection velocity, D_{pp} is the momentum diffusion coefficient and q is the source power density. This equation is numerically solved with the GALPROP code `v50.1p` in two dimensions, that is assuming azimuthal symmetry around the galactic centre and enforcing the boundary condition $n \equiv 0$ on a cylinder of radius $R = 20\,\mathrm{kpc}$ and half-height z_{max} (see below).

The source power density q factorises into a source energy spectrum $q_0 E^{-\alpha}$ and a spatial variation $\sigma(r)\mathrm{e}^{-z/z_{\mathrm{scale}}}$ with $z_{\mathrm{scale}} = 0.2\,\mathrm{kpc}$. For the radial part we consider two possibilities. The distribution of SNRs is expected to be correlated with that of pulsars which is inferred by Lorimer to be [26]

$$\sigma_{\mathrm{Lorimer}}(r) = 64.6 \left(\frac{r}{\mathrm{kpc}} \right)^{2.35} \mathrm{e}^{-r/1.528\,\mathrm{kpc}}\,. \tag{3.1}$$

However, the determination of pulsar distances from their rotation measures relies on knowledge of the thermal electron density throughout the Galaxy and different distributions

lead to different functional forms for the inferred radial variation of the pulsar density [27]. Therefore we also consider an exponential source distribution

$$\sigma_{\rm exp}(r) = \sigma_0 {\rm e}^{-r/2\,{\rm kpc}}\,, \tag{3.2}$$

following Refs.[28] and [29].

The normalisation D_{0xx}, the scale height $z_{\rm max}$ of the CR halo and the spectral index δ of the diffusion coefficient are usually determined from measurements of CR nuclei and nuclear secondary to primary ratios. The measurement of CR 'chronometers' like ^{10}Be/^{9}Be is still not precise enough to break the degeneracy between D_{0xx} and $z_{\rm max}$, so we vary $z_{\rm max}$ between 4 kpc and 8 kpc and vary D_{0xx} only a little, checking that we have rough agreement with the measured fluxes of nuclei and nuclear secondary-to-primary ratios. On theoretical grounds [30] one expects a spectral break in the diffusion coefficient at ≈ 1 GeV. We fix the break energy to 1 GeV and vary δ_1 and δ_2 below and above the break (keeping $\delta_1 \geq \delta_2$), again trying to satisfy all local CR measurements.

The source electron spectrum is usually assumed to have a break around 4 GeV [31] so we fix the electron source normalisation $q_0\sigma_0$ and the spectral indices α_1 and α_2 below and above the break by fitting the propagated flux to the electron spectrum as measured at Earth [32, 33]. We apply Solar modulation in the spherical approximation [34] with a median potential of $\phi = 550$ MV. Reacceleration and convection play a role at energies below 10 GeV and are therefore important for the 408 MHz map. For the Alfvèn velocity $v_{\rm A}$ which determines the strength of reacceleration via $D_{pp} \propto v_{\rm A}^2$ we consider the range $0-50\,{\rm km\,s^{-1}}$. `GALPROP` assumes the convection velocity to vary linearly with distance from the galactic plane and we vary the slope ${\rm d}v_{\rm conv}/{\rm d}z$ between 0 and $20\,{\rm km\,s^{-1}\,kpc^{-1}}$.

Since the random component of the galactic magnetic field is known to dominate over the regular component [35], we neglect the latter. For the radial dependence we adopt the usual exponential fall-off where the radial scale ρ and the (perpendicular component of the) field strength B_0 at the galactic centre are chosen to reproduce the 408 MHz skymap [36]. Although it was initially believed [37] that an exponential dependence on z could give a satisfactory fit to the 408 MHz latitude profile, the galactic field model was later refined

	Lorimer	exponential
Source distribution	*c.f.* eq. 3.1	*c.f.* eq. 3.2
α_1, α_2	1.2, 2.2	1.2, 2.2
D_{0xx}	$5.75 \times 10^{28}\,{\rm cm^2\,s^{-1}}$	$5.75 \times 10^{28}\,{\rm cm^2\,s^{-1}}$
$z_{\rm max}$	4 kpc	8 kpc
δ_1, δ_2	0.34, 0.34	0.1, 0.4
$v_{\rm A}$	$50\,{\rm km\,s^{-1}}$	$36\,{\rm km\,s^{-1}}$
${\rm d}v_{\rm conv}/{\rm d}z$	$10\,{\rm km\,s^{-1}\,kpc^{-1}}$	$15\,{\rm km\,s^{-1}\,kpc^{-1}}$
B_0	$6.3\,\mu$G	$6.8\,\mu$G
ρ	5 kpc	50 kpc

Table 1: Parameters of source and diffusion models.

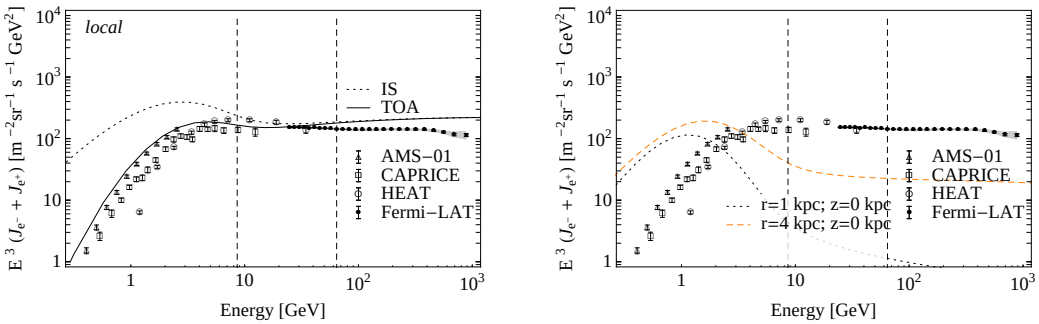

Figure 1: Left panel. The electron (plus positron) flux measured locally by AMS-01, CAPRICE, HEAT [32] and Fermi-LAT [33], compared with the expectation for the Lorimer source distribution (3.1); the dotted line is the calculated interstellar (IS) flux while the solid line is its Solar modulated (TOA) value (with $\phi = 550$ MV). The dashed vertical lines show the energy corresponding to peak synchrotron frequencies of 408 MHz and 23 GHz for the local magnetic field. **Right panel.** The calculated electron (plus positron) flux at the positions $\{(r, z)\} = \{(1, 0), (4, 0))\}$ (in kpc).

[38] by considering different, non-exponential behaviours which in fact give better fits. We therefore apply the method described in Ref. [39] of determining the emissivity dependence on r for galactic longitude $\ell = \pm 180°$ (towards the galactic anti-centre). With an estimate for the electron density this translates into a z-dependence of the form $a + b \exp\left[(-|z|/\xi)^{\kappa}\right]$ and this is iterated to convergence where we find $a/b = 0.27$, $\xi = 0.51$ and $\kappa = 0.68$.

4. Results

4.1 Lorimer source distribution

The parameters of the diffusion model, the magnetic field and the electron source spectrum have been adjusted as described above and the values are shown for the Lorimer source distribution (3.1) in Table 1. Almost all diffusion model parameters are in the range also found by previous `GALPROP` studies [37, 31, 30] to give a consistent picture of GCRs. The only difference is the electron injection spectrum which is chosen considerably harder to reproduce the new measurement by Fermi-LAT at $\mathcal{O}(100)$ GeV energies which was not available for the above mentioned studies.

The electron flux measured locally and at the positions $\{(r, z)\} = \{(1, 0), (4, 0)\}$ (in kpc) are shown in Fig. 1. We note that close to the galactic centre the electron flux responsible for synchrotron radiation at 408 MHz is not only much softer but also suppressed by over an order of magnitude with respect to its locally measured value. The predicted local electron flux seems to be too hard at energies above tens of GeV and overshoots the measurement by Fermi-LAT. We note however that this is only an effect of the assumed *continuous* source distribution as implemented in the `GALPROP` code by default. At energies $\mathcal{O}(100)$ GeV, however, where the diffusion-loss length of electrons $\ell(E)$ becomes smaller than the distance between the solar system and the nearest source(s), the discreteness of GCR sources starts to play a role, leading to a cut-off in the power law local electron spectrum (see [12] for an illustration of this effect). We note that the locally measured electron

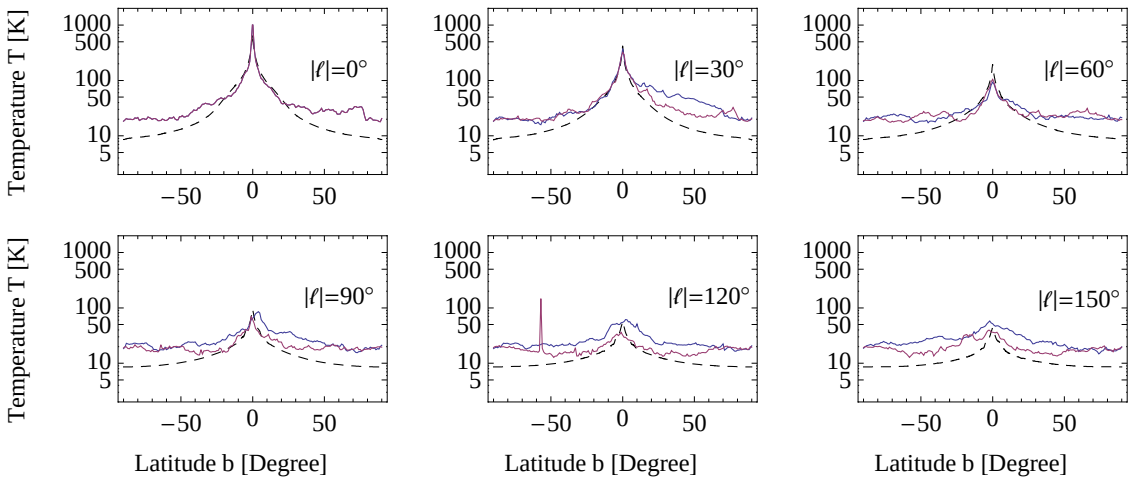

Figure 2: The calculated latitudinal profile of galactic synchrotron radiation at 408 MHz (black dashed line) for galactic longitudes $|\ell| = 0°, 30°, 60°, 90°, 120°$ and 150°. The red (blue) solid line is the observed profile [36] for positive (negative) ℓ.

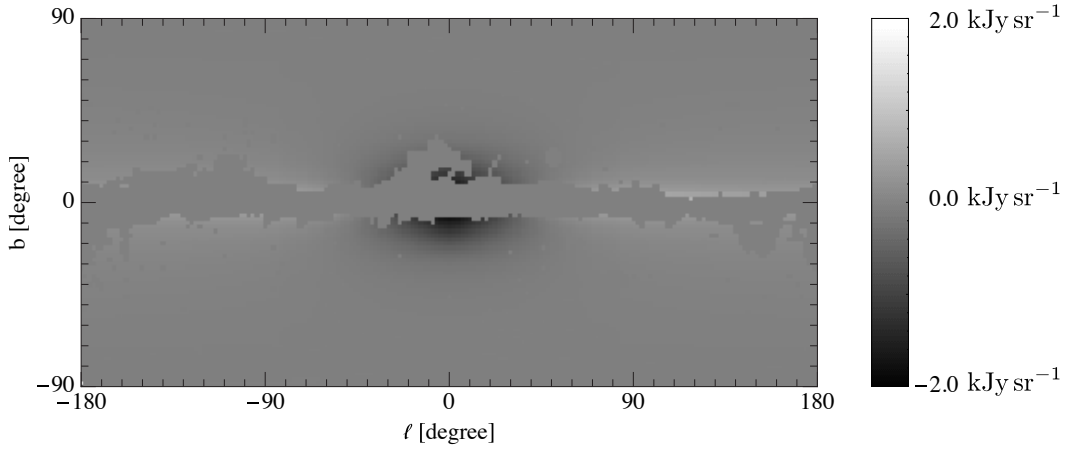

Figure 3: Residual skymap in galactic coordinates for the Lorimer source distribution (3.1).

spectrum (from a discrete distribution of sources) does in fact correspond to a power law spectrum $\propto E^{-3}$ or slightly harder. This is in agreement with the spectrum predicted from both our source distributions and injection spectra.

Fig. 2 shows the latitudinal profiles of the synchrotron radiation at 408 MHz; in general, the fit is good for $b \lesssim 50°$ but underestimates the emission at larger latitudes. It has been shown [39] that this can potentially be overcome by increasing the scale height of the synchrotron emissivity at larger galactic radii. The remaining discrepancies between the simulated and measured profiles are probably due to the assumption of rotational symmetry. This leads to an underestimation of the synchrotron radiation along tangents of the spiral arms and an overestimation between them. For example, the Carina arm

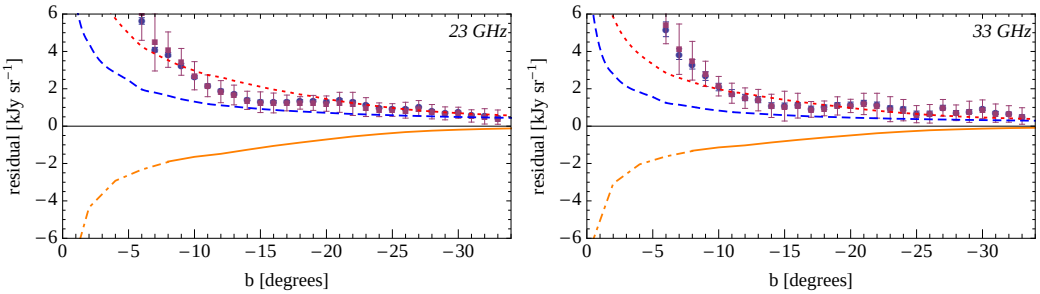

Figure 4: Latitudinal profile of the K band residual outside (solid curve) and under (dot-dashed curve) the mask at 23 GHz (left panel) and 33 GHz (right panel) for $\ell = 0$. The square (circle) data points are the 'haze' as extracted in Ref. [3] ([8]). The dotted line shows the extrapolated emission at 23 (33) GHz from scaling the simulated 408 MHz emission and the dashed line shows the actual simulated 23 (33) GHz emission.

is tangent at 75° and the Sagittarius arm at −40°, so both $\ell = +60°$ and $\ell = -60°$ are between spiral arms and thus slightly overestimated, in particular in the galactic plane. It is also clear that point sources (that have not been subtracted from the 408 MHz data) are not accounted for in our calculation (*e.g.,* Fornax at $\ell \simeq 120°$, $b \simeq -57°$).

The skymap of the residual $r(\ell, b)$ (Fig. 3) shows a deficit for $|\ell| \leq 40°$ and $|b| \leq 20°$. Further away from the galactic centre direction there is a slight excess. The residual specific intensity (Fig. 4) is of opposite sign but its absolute value is of the same order of magnitude as the 'haze' at 23 and 33 GHz. Such *intrinsic* residuals of the template subtraction can substantially modify the magnitude, morphology and/or spectrum of any *physical* residual that might be present in the microwave data. We emphasise that this will have important consequences for the allowed parameter space of models trying to explain such a potential excess, for example by dark matter annihilation.

4.2 Exponential source distribution

For the exponential source distribution (3.2), the electron fluxes are shown in Fig. 5. Close to the galactic centre, it is larger by about an order of magnitude than measured locally and slightly harder. The latitudinal profiles of the synchrotron radiation at 408 MHz are shown in Fig. 6.

The residual skymap contains a roughly spherical excess around the centre of the map, although somewhat more extended in longitude than in latitude (see Fig. 7).

We note that the systematic uncertainty of the residual intensity (as determined from real skymaps) induced by chance correlations between the 'haze' template and the CMB has been estimated in Ref. [3] and can be read off their Fig. 8 as $\pm 11.8\,\mathbf{h}\,\mathrm{kJy\,sr^{-1}}$ ($\pm 23.7\,\mathbf{h}\,\mathrm{kJy\,sr^{-1}}$) in the 23 GHz (33 GHz) band. We therefore allow for an offset of our calculated residual relative to the 'haze' template in this range when fitting the residuals from real skymaps. The residual intensity (Fig. 8) *matches* the claimed WMAP haze in latitudinal profile.

To compare our results to those of Ref. [3], we also determine the average spectral index (for details see Appendix A) in a region south of the galactic centre, $b \in [-45°, 0°]$, $\ell \in$

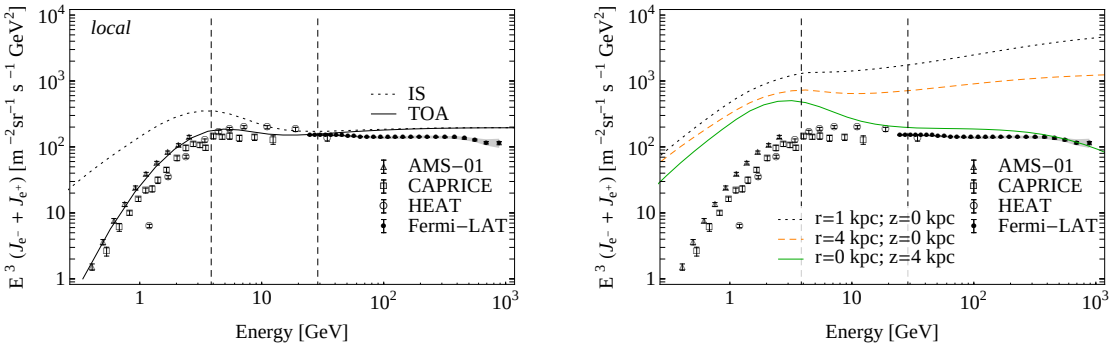

Figure 5: Same as in Fig. 1, but for the exponential source distribution (3.2).

$[-25°, 25°]$. The colour maps of spectral indices scaled by intensity are shown in Fig. 9, both for the synchrotron + residual and for the residual alone. Not only is the synchrotron emission much more disk-like than the residual, but the spectral index of the residual is also considerably harder than the synchrotron spectral index. This is to be compared with Fig. 7 of Ref. [3] which exhibits the same qualitative behaviour.

Furthermore, we show the spectral index for the unmasked pixels in the region south of the galactic centre (as defined above) as a function of latitude in Fig. 10, again both for the synchrotron + residual and for the residual alone. With average indices of $\langle \beta^{\mathrm{H}}_{23,33} \rangle = -0.44$ for the residual and of $\langle \beta^{\mathrm{S}}_{23,33} \rangle = -1.03$ for the residual + synchrotron in this region, we find that the residual index is harder than the synchrotron index by 0.6, which is in excellent agreement with the findings of Ref. [3]. The values of our different model parameters are shown in Table 1.

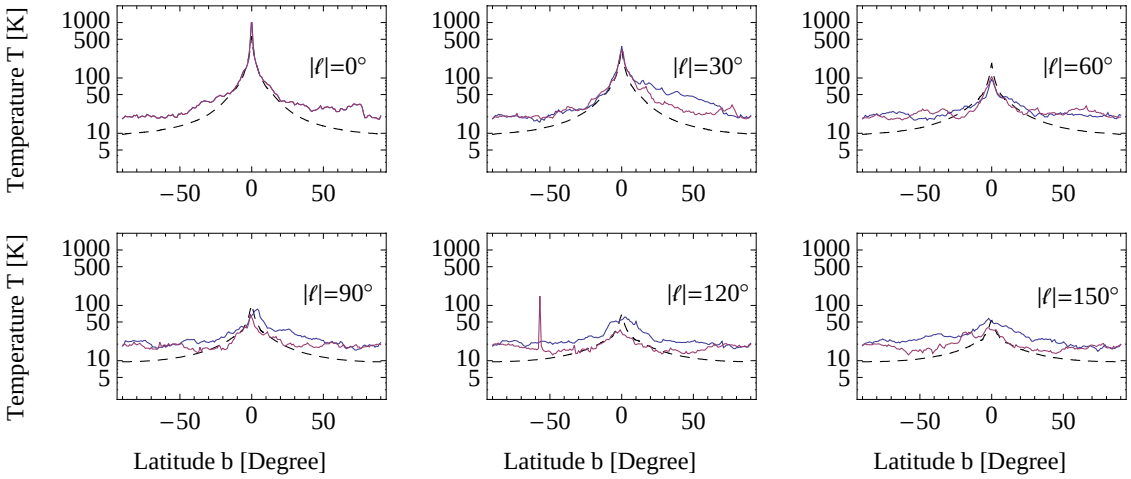

Figure 6: Same as in Fig. 2, but for the exponential source distribution (3.2).

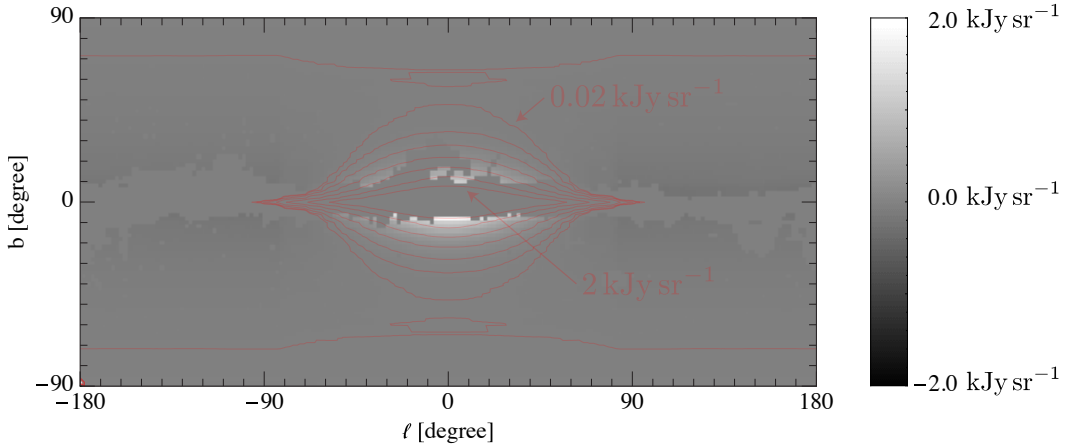

Figure 7: Residual skymap in galactic coordinates for the exponential source distribution (3.2). The contour lines are equally spaced between $0.02\,\mathrm{kJy\,sr^{-1}}$ and $2\,\mathrm{kJy\,sr^{-1}}$.

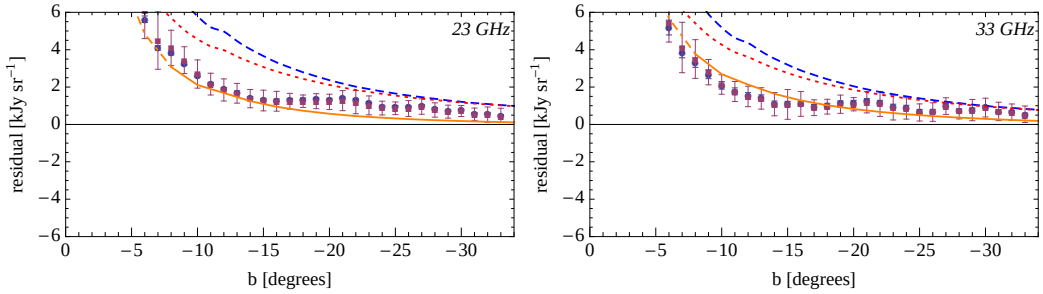

Figure 8: Same as in Fig. 4, but for the exponential source distribution (3.2). We have added an offset to the calculated residual of $+11.8\,\mathbf{h}\,\mathrm{kJy\,sr^{-1}}$ ($+23.7\,\mathbf{h}\,\mathrm{kJy\,sr^{-1}}$) in the 23 GHz (33 GHz) band reflecting the systematic uncertainty from chance correlations between the 'haze' template and the CMB.

5. Discussion

To qualitatively understand these results, we consider the longitudinal and latitudinal profiles of the synchrotron intensity $I(\ell, b)$; for simplicity let us constrain ourselves to the galactic plane, *i.e.*, $z \equiv 0$ and a plane perpendicular, *i.e.*, $r \equiv 0$. The intensity in any direction ℓ, b is given by the integral of the synchrotron emissivity over the line of sight and this samples the radial distribution of the relativistic electron density in the range $r \in [d \sin \ell,\ R]$ and $z \in [0, \min[z_{\max}, (d + R) \tan b]]$, where d is the distance of the Sun from the galactic centre. Since the fitting procedure minimises the square of the difference in the maps, the sign and size of the residual is determined not by the absolute difference but by the difference in the *slopes* in r and z of the emissivity $\varepsilon(r, z)$ at 408 MHz and the WMAP frequencies. The difference in the slopes reflects the energy dependence of the electron diffusion — higher energy electrons lose their energy more quickly, hence their emissivity traces the source distribution more closely than does the emissivity of low energy electrons.

Considering the galactic plane ($z \equiv 0$) first, for the pulsar source distribution the

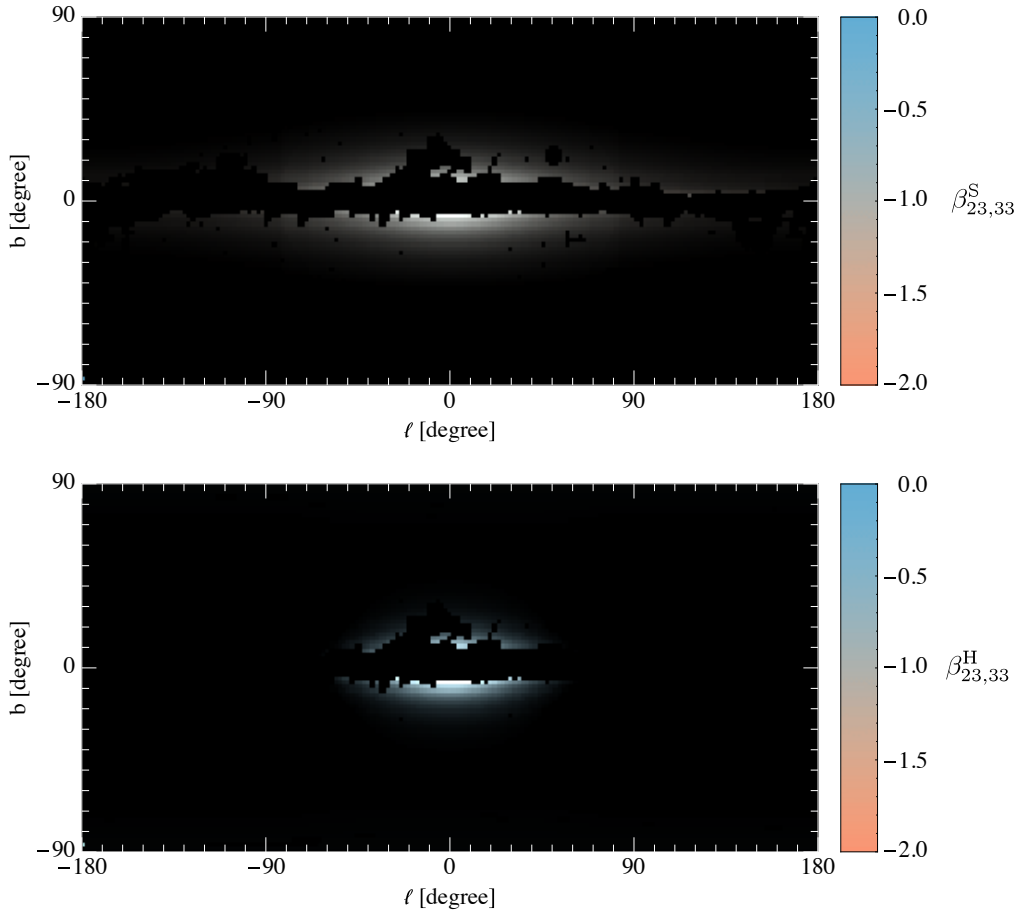

Figure 9: Colour maps of spectral indices between 23 and 33 GHz defined in eq. A.1 scaled by the 23 GHz intensity for synchrotron + residual (top panel) and residual only (bottom panel).

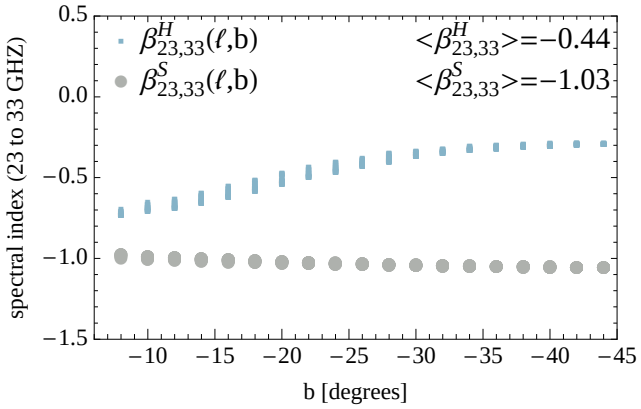

Figure 10: Spectral indices of the unmasked pixels in the region south of the galactic centre ($b \in [-45°, 0°]$, $\ell \in [-25°, 25°]$) as a function of latitude for residual + synchrotron (large beige circles) and residual alone (small blue squares). The average spectral indices, $\beta_{\rm S}$ and $\beta_{\rm H}$, are shown in the upper right corner.

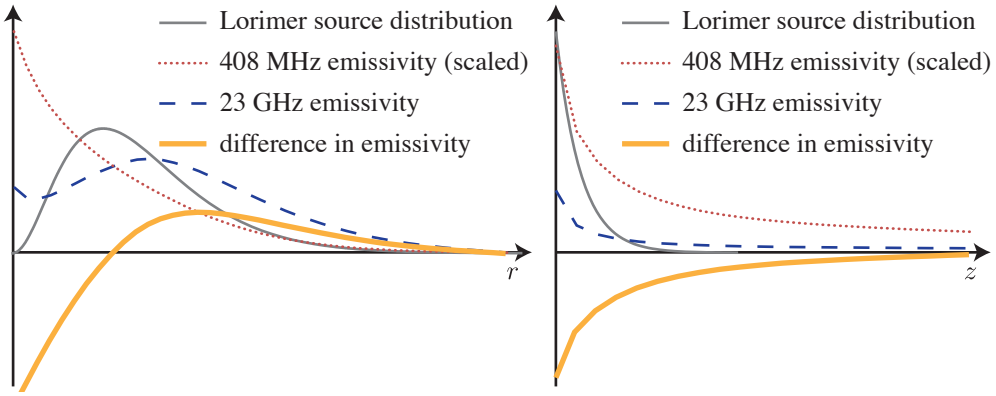

Figure 11: The (scaled) synchrotron emissivity at 408 MHz and 23 GHz, and their difference for the Lorimer type source distribution at $z = 0\,\mathrm{kpc}$ (left) and $r = 0\,\mathrm{kpc}$ (right).

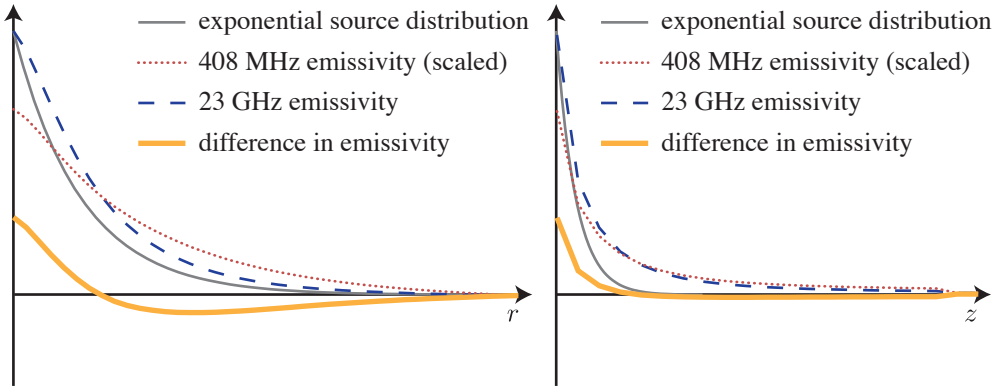

Figure 12: Same as Fig. 11 but for the exponential source distribution.

low energy electrons peak at the galactic centre whereas the high-energy electrons peak further away along the galactic plane (see Fig. 11). This leads to a deficit for small radii (translating to small longitudes) and a slight excess further away from the galactic centre (see also Fig. 3). For the exponential source distribution the radial distribution of synchrotron emissivity is steeper at higher energies. The template subtraction therefore yields a residual with an excess around the centre direction and a deficit further away along the galactic plane (see Fig. 12).

Perpendicular to the galactic plane ($r \equiv 0$), the slope of the emissivities of low and high energy electrons is similar for both models, since the z-dependence of the source distributions is the same. However, due to the different variation with galacto-centric radius, the relative normalisations $\mathbf{a}$ (see Sec. 2), which are influenced by the larger number of pixels off the galactic centre direction, *are* different. Therefore the residual is negative for the Lorimer source distribution and positive for the exponential source distribution.

We note that the size and morphology of the residual is thus sensitive not only to the source distribution but also to the parameters of the diffusion model. For instance, decreasing the Alfvèn speed below the value given above reduces the importance of reac-

celeration, and therefore effectively limits the number of GeV electrons around the galactic centre where otherwise energy losses dominate.

6. Conclusion

We have investigated systematic effects in WMAP foreground subtraction stemming from the naïve extrapolation of the 408 MHz map. To this end we have considered two illustrative cosmic ray diffusion models assuming different source distributions, the first one based on a pulsar survey, and the second one exponential in galacto-centric radius. Both models are able to reproduce the synchrotron radiation at 408 MHz, the locally measured electron flux and are furthermore consistent with nuclear cosmic ray fluxes and secondary-to-primary ratios. When our 'foreground' 408 MHz map is subtracted from the 23 GHz map, we find a residual whose size and morphology depends on the source and diffusion model adopted. Thus the energy-dependent diffusion of relativistic electrons makes the 408 MHz skymap a *bad* tracer of synchrotron radiation at microwave frequencies, as had been suspected earlier [41]. Such a template subtraction produces a residual of the same overall intensity as the haze and can for particular source distributions give the same latitudinal profile.

For the Lorimer source distribution, the residual is of *opposite* sign to the "haze" and can therefore certainly not explain the "haze" as a residual of the template subtraction. However since it is of comparable magnitude and its morphology is strikingly similar, it is important to keep this issue in mind when interpreting the "haze" as an excess over standard synchrotron emission from electrons injected by SNRs. We emphasise that the significant uncertainty thus introduced has a considerable effect on the parameter space available for possible explanations of the "haze", *e.g.,* dark matter annihilation or pulsars.

The residual obtained from the exponential source distribution does not perfectly reproduce the morphology found in Ref. [3] (although it is *not* disk-like but rather clustered around the galactic centre). However, a quantitative assessment of the discrepancy is not straightforward, mainly because Ref. [3] does not provide any objective measure, *e.g.,* the ellipticity of equal intensity contours. On the other hand, even the numerical `GALPROP` model we employed for our analysis is very likely too simple to fully capture the complexity of synchrotron emission in the Galaxy. For instances, not only the source density but also the galactic magnetic field is supposed to be correlated with the galactic spiral arms, which will break the symmetry in r (and hence in ℓ) and can therefore considerably modify the morphology. Furthermore, much of the 'diffuse' synchrotron emission from the disk may originate in the shells of old supernova remnants which have grown very large in their radiative phase [42]. Exactly the same argument concerning the energy-dependent diffusion length that we applied to the cosmic ray source distribution can be applied to such localised structures too. Therefore the 408 MHz survey skymap is not expected to trace the emission from the latter at higher frequencies either. One can easily imagine that such localised structures (of which Loop I is a nearby example) might at least in part modify the morphology of the residual and bring the simulated map into agreement with the one determined from the subtraction of real templates.

Note added

As we were about to submit this manuscript, a related study appeared [43]. Although we agree on the importance of diffusion-loss steepened electron spectra for producing the haze there is a major difference between our approaches — while the authors of Ref. [43] consider the haze to be *physical*, we argue that it might in fact be an artifact of the foreground subtraction. Our models are also more constrained insofar as we reproduce the observed radio emission at 408 MHz and match the direct measurements of the electron spectrum at our position. Furthermore, we allow for spatial dependence of the **B** field, and convection and reacceleration of cosmic ray electrons, which are all essential in order explain all these datasets simultaneously.

6.1 Acknowledgements

PM acknowledges support by the EU Marie Curie Network "UniverseNet" (HPRN-CT-2006-035863) and a STFC Postgraduate Studentship.

A. Determination of the spectral index

In general, a spectral index $\beta(\mathbf{x})$ between two different frequencies, ν_1 and ν_2, can be defined for each given pixel $\mathbf{x}$ by assuming a power law behaviour of the specific intensity, $I(\nu, \mathbf{x})$:

$$\frac{I(\nu_2, \mathbf{x})}{I(\nu_1, \mathbf{x})} = \left(\frac{\nu_2}{\nu_1}\right)^{\beta(\mathbf{x})} . \tag{A.1}$$

However, it turns out that the template method applied to the WMAP data and the 408 MHz skymap leads to a residual with *negative* intensities for some pixels (see, *e.g.*, Fig. 6 of Ref. [3]), partly due to over-subtraction and partly because the skymaps are mean-subtracted. We also find negative intensities for some pixels when applying the template subtraction to our mock microwave data and radio template. This does not necessarily imply that the residual is not physical but that a global offset $\Delta I(\nu)$ exists between the residual intensity, I', as determined from the template subtraction and the intensity of the *actual,* possibly physical residual, I:

$$\Delta I(\nu) \equiv I(\nu, \mathbf{x}) - I'(\nu, \mathbf{x}) . \tag{A.2}$$

This makes the determination of the spectral index non-trivial.

At first sight, the analysis presented in Ref. [3] seems to avoid this difficulty by determining the average spectral index in the region south of the galactic centre from the average ratio r' of the intensities at two different frequencies ν_1 and ν_2, *e.g.,* $\nu_1 = 23\,\mathrm{GHz}$ and $\nu_2 = 33\,\mathrm{GHz}$. This ratio can be determined from a scatter plot of the pairs of residual intensities $\{I'_{\nu_1}, I'_{\nu_2}\}$ (as determined from the template subtraction), to which a straight line, $I'_{\nu_2}(I'_{\nu_1}) = r' I'_{\nu_1} + \hat{I}'_{\nu_2}$, is fitted, allowing for the ordinate offset $\hat{I}'_{\nu_2}$ because of the unknown global offset $\Delta I(\nu)$. The average spectral index $\langle \beta'_{\nu_1,\nu_2} \rangle$ defined by this procedure is then simply $\log(r')/\log(\nu_2/\nu_1)$. Alternatively, if the spectral index is determined from a scatter plot of the *actual* residual intensities $\{I_{\nu_1}, I_{\nu_2}\}$, then there is no ordinate offset,

so the straight line is $I_{\nu_2}(I_{\nu_1}) = rI_{\nu_1}$ and the *actual* average spectral index $\langle\beta_{\nu_1,\nu_2}\rangle = \log(r)/\log(\nu_2/\nu_1)$.

In general, these two descriptions cannot be expected to give a similar spectral index. Even assuming that with an appropriate 'haze' template $\mathbf{h}$ the amount of over-subtraction is much smaller than the offset due to the use of mean-subtracted maps, the answer is in general different. In this case, the offset is simply the mean over the n pixels, $\Delta I(\nu) = \langle I(\nu, \mathbf{x})\rangle$. The coordinate system $\{I'_{\nu_1}, I'_{\nu_2}\}$ is therefore centred at the centre of gravity of the data $\{I(\nu_1, \mathbf{x}), I(\nu_2, \mathbf{x})\}$, and the ordinate offset $\hat{I}'_{\nu_2}$ is zero. As usual, the slope of the linear regression $I'_{\nu_2}(I'_{\nu_1}) = r' I'_{\nu_1}$ is

$$r' = \frac{\sum_i I'_{\nu_1}(\mathbf{x}_i) I'_{\nu_2}(\mathbf{x}_i) - n\langle I'_{\nu_1}(\mathbf{x}_i)\rangle\langle I'_{\nu_2}(\mathbf{x}_i)\rangle}{\sum_i I'^2_{\nu_1}(\mathbf{x}_i) - n\langle I'_{\nu_1}(\mathbf{x}_i)\rangle^2} \,. \tag{A.3}$$

Unless the covariance of I'_{ν_1} and I'_{ν_2} is much larger than the product of their mean values, which is for example the case if the spectral index is constant in the region of interest, this is in general different from the slope r of the straight line $I_{\nu_2}(I_{\nu_1}) = rI_{\nu_1}$,

$$r = \frac{\sum_i I'_{\nu_1}(\mathbf{x}_i) I'_{\nu_2}(\mathbf{x}_i)}{\sum_i I'^2_{\nu_1}(\mathbf{x}_i)} \,. \tag{A.4}$$

However, since we cannot determine the offset $\Delta I(\nu)$ from data, we need to *define* an offset $\Delta I(\nu)$. We choose it to be:

$$\Delta I(\nu) = \min_{\mathbf{x}} \left[I'(\nu, \mathbf{x})\right] \,, \tag{A.5}$$

such that the intensity is always positive, allowing us to define the spectral index in each pixel. (The exact value chosen for $\Delta I(\nu)$ is actually $(1 + 10^{-3}) \min\left[I'(\nu, \mathbf{x})\right]$ to prevent the spectral index from diverging in the pixel where $I(23\,\mathrm{GHz})$ is minimum.)

References

[1] J. Dunkley *et al.*, arXiv:0811.3915 [astro-ph].

[2] D. P. Finkbeiner, *Astrophys. J.* **614** (2004) 186.

[3] G. Dobler and D. P. Finkbeiner, *Astrophys. J.* **680** (2008) 1222.

[4] M. Bottino, A. J. Banday and D. Maino, *Mon. Not. R. Astron. Soc.* **402** (2010) 207.

[5] C. Dickinson *et al.*, *Astrophys. J.* **705** (2009) 1607..

[6] D. T. Cumberbatch, J. Zuntz, H. K. K. Eriksen and J. Silk, arXiv:0902.0039 [astro-ph.GA].

[7] D. P. Finkbeiner, arXiv:astro-ph/0409027.

[8] D. Hooper, D. P. Finkbeiner and G. Dobler, *Phys. Rev.* **D 76** (2007) 083012.

[9] M. Kaplinghat, D. J. Phalen and K. M. Zurek, *J. Cosmo. Astropart. Phys.* **12** (2009) 010.

[10] J. P. Harding and K. N. Abazajian, *Phys. Rev.* **D 81** (2010) 023505.

[11] P. Blasi, *Phys. Rev. Lett.* **103** (2009) 051104.

[12] M. Ahlers, P. Mertsch and S. Sarkar, *Phys. Rev.* **D 80** (2009) 123017.

[13] O. Adriani *et al.* [PAMELA Collaboration], *Nature* **458** (2009) 607.

[14] G. Dobler, D. P. Finkbeiner, I. Cholis, T. R. Slatyer and N. Weiner, arXiv:0910.4583 [astro-ph.HE].

[15] W. B. Atwood *et al.* [Fermi-LAT Collaboration], *Astrophys. J.* **697** (2009) 1071.

[16] T. Linden and S. Profumo, arXiv:1003.0002.

[17] A. A. Abdo *et al.* [Fermi-LAT collaboration], *Phys. Rev. Lett.* **104** (2010) 101101.

[18] J. M. Casandjian, I. Grenier and f. t. F. Collaboration, arXiv:0912.3478.

[19] B. Gold *et al.*, arXiv:1001.4555 [astro-ph.GA].

[20] A. de Oliveira-Costa, M. Tegmark, R. D. Davies, C. M. Gutierrez, A. N. Lasenby, R. Rebolo and R. A. Watson, Astrophys. J. **606** (2004) L89 [arXiv:astro-ph/0312039].

[21] B. T. Draine and A. Lazarian, Astrophys. J. **508** (1998) 157 [arXiv:astro-ph/9802239].

[22] A. W. Strong, I. V. Moskalenko and V. S. Ptuskin, *Ann. Rev. Nucl. Part. Sci.* **57** (2007) 285.

[23] E. M. Berkhuijsen, *Astron. Astrophys.* **14** (1971) 359.

[24] I. V. Moskalenko and A. W. Strong, *Astrophys. J.* **493** (1998) 694.

[25] V. L. Ginzburg, V. A. Dogiel, V. S. Berezinsky, S. V. Bulanov and V. S. Ptuskin, "Astrophysics of cosmic rays" (Amsterdam: North-Holland, 1990) 534 p.

[26] D. R. Lorimer, in IAU Symposium, Vol. 218, "Young Neutron Stars and Their Environments", ed. F. Camilo & B. M. Gaensler, p.105.

[27] D. R. Lorimer *et al.*, *Mon. Not. R. Astron. Soc.* **372** (2006) 777.

[28] B. Paczynksi, *Astrophys. J.* **348** (1990) 485.

[29] S. J. Sturner and C. D. Dermer, *Astrophys. J.* **461** (1996) 872.

[30] V. S. Ptuskin, I. V. Moskalenko, F. C. Jones, A. W. Strong and V. N. Zirakashvili, Astrophys. J. **642** (2006) 902 [arXiv:astro-ph/0510335].

[31] A. W. Strong, I. V. Moskalenko, and O. Reimer, Astrophys. J. **613** (2004) 962–976, [arXiv:astro-ph/0406254].

[32] A. W. Strong and I. V. Moskalenko, arXiv:0907.0565 [astro-ph.HE].

[33] A. A. Abdo *et al.* [Fermi LAT Collaboration], *Phys. Rev. Lett.* **102** (2009) 181101.

[34] L. J. Gleeson, W. I. Axford, *Astrophys. J.* **154** (1968) 1011.

[35] R. Beck, arXiv:0812.4925 [astro-ph].

[36] C. G. T. Haslam, C. J. Salter, H. Stoffel and W. E. Wilson, *Astron. Astrophys.* **47** (1982) 1.

[37] A. W. Strong, I. V. Moskalenko and O. Reimer, Astrophys. J. **537** (2000) 763 [Erratum-ibid. **541** (2000) 1109] [arXiv:astro-ph/9811296].

[38] E. Orlando, A. W. Strong, I. V. Moskalenko, T. A. Porter, G. Johannesson and S. W. Digel, arXiv:0907.0553 [astro-ph.GA].

[39] S. Philipps, S. Kearsey, J. L. Osborne, C. G. T. Haslam and H. Stoffel, *Astron. Astrophys.* **103** (1981) 405.

[40] T. Kobayashi, Y. Komori, K. Yoshida and J. Nishimura, *Astrophys. J.* **601** (2004) 340.

[41] C. Bennett *et al.* [WMAP Collaboration], *Astrophys. J. Suppl.* **148** (2003) 97.

[42] S. Sarkar, *Mon. Not. R. Astron. Soc.* **199** (1982) 97.

[43] M. McQuinn and M. Zaldarriaga, arXiv:1004.1189 [astro-ph.HE].